



Discovery of Three New Transiting Hot Jupiters: WASP-161 b, WASP-163 b, and WASP-170 b

K. Barkaoui^{1,2}, A. Burdanov¹, C. Hellier³, M. Gillon¹, B. Smalley³, P. F. L. Maxted³, M. Lendl^{4,5},
A. H. M. J. Triaud⁶, D. R. Anderson³, J. McCormac⁷, E. Jehin¹, Y. Almléay^{8,9}, D. J. Armstrong⁷, Z. Benkhaldoun²,
F. Bouchy⁵, D. J. A. Brown⁷, A. C. Cameron¹⁰, A. Daassou², L. Delrez^{1,11}, E. Ducrot¹, E. Foxell⁷, C. Murray¹¹, L. D. Nielsen⁵,
F. Pepe⁵, D. Pollacco⁷, F. J. Pozuelos¹, D. Queloz^{5,11}, D. Segransan⁵, S. Udry⁵, S. Thompson¹¹, and R. G. West⁷

¹Space Sciences, Technologies and Astrophysics Research (STAR) Institute, Université de Liège, Belgium; khalid.barkaoui@doct.uliege.be

²Oukaimeden Observatory, High Energy Physics and Astrophysics Laboratory, Cadi Ayyad University, Marrakech, Morocco

³Astrophysics Group, Keele University, Staffordshire, ST5 5BG, UK

⁴Space Research Institute, Austrian Academy of Sciences, Schmiedlstr. 6, A-8042 Graz, Austria

⁵Observatoire astronomique de l'Université de Genève, 51 ch. des Maillettes, 1290 Sauverny, Switzerland

⁶School of Physics and Astronomy, University of Birmingham, Edgbaston, Birmingham B15 2TT, UK

⁷Department of Physics, University of Warwick, Gibbet Hill Road, Coventry, CV4 7AL, UK

⁸Space and Astronomy Department, Faculty of Science, King Abdulaziz University, 21589 Jeddah, Saudi Arabia

⁹King Abdullah Centre for Crescent Observations and Astronomy, Makkah Clock, Mecca 24231, Saudi Arabia

¹⁰School of Physics and Astronomy, University of St. Andrews, North Haugh, St. Andrews, Fife KY16 9SS, UK

¹¹Cavendish Laboratory, J J Thomson Avenue, Cambridge, CB3 0HE, UK

Received 2018 July 15; revised 2018 November 21; accepted 2018 November 25; published 2019 January 11

Abstract

We present the discovery of three new transiting hot Jupiters by the WASP-South project, WASP-161 b, WASP-163 b, and WASP-170 b. Follow-up radial velocities obtained with the Euler/CORALIE spectrograph and transit light curves obtained with the TRAPPIST-North, TRAPPIST-South, SPECULOOS-South, NITES, and Euler telescopes have enabled us to determine the masses and radii for these transiting exoplanets. WASP-161 b completes an orbit around its $V = 11.1$ F6V-type host star in 5.406 days, and has a mass $M_p = 2.5 \pm 0.2 M_{\text{Jup}}$ and radius $R_p = 1.14 \pm 0.06 R_{\text{Jup}}$. WASP-163 b orbits around its host star (spectral type G8V and the magnitude $V = 12.5$) every 1.609 days, and has a mass of $M_p = 1.9 \pm 0.2 M_{\text{Jup}}$ and a radius of $R_p = 1.2 \pm 0.1 R_{\text{Jup}}$. WASP-170 b has a mass of $1.7 \pm 0.2 M_{\text{Jup}}$ and a radius of $1.14 \pm 0.09 R_{\text{Jup}}$ and is on a 2.344 day orbit around a G1V-type star of magnitude $V = 12.8$. Given their irradiances ($\sim 10^9 \text{ erg s}^{-1} \text{ cm}^{-2}$) and masses, the three new planets' sizes are in good agreement with classical models of irradiated giant planets.

Key words: planetary systems – techniques: photometric – techniques: radial velocities – techniques: spectroscopic

1. Introduction

Inaugurated by the seminal discovery of 51 Peg b in 1995 (Mayor & Queloz 1995), the study of exoplanets has dramatically developed to become one of the most important fields of modern astronomy. Since 1995, most of the exoplanets have been detected by the transit technique (Charbonneau et al. 2000; Henry et al. 2000).

Among this large harvest, highly irradiated giant planets (a.k.a. hot Jupiters) transiting bright nearby stars have a particular scientific interest. These rare objects— $<1\%$ of solar-type stars (Winn & Fabrycky 2015)—undergo irradiation that is orders of magnitude larger than that of any solar system planet (Fortney et al. 2007), and are subject to intense gravitational and magnetic fields (Chang et al. 2010; Correia & Laskar 2010). Studying in detail their physical and chemical responses to such extreme conditions provides a unique opportunity to improve our knowledge on planetary structure, composition, and physics. The brightness of their host star combined with their eclipsing configuration makes such detailed characterization possible, notably to precisely measure their size, mass, and orbital parameters (Deming & Seager 2009; Winn 2010), but also to probe their atmospheric properties, for example, the $P - T$ profiles, chemical composition, and albedos (Seager & Deming 2010; Crossfield 2015; Sing et al. 2016).

The WASP (Wide Angle Search for Planets) project (described in Pollacco et al. 2006; Collier Cameron et al. 2007) uses two

robotic installations, one at La Palma (Spain) and one at Sutherland (South Africa), to scout the sky for gas giants transiting the solar-type stars. With more than 100 hot Jupiters discovered so far in front of bright nearby stars, WASP is a key contributor to the study of highly irradiated giant planets. In this paper, we report the discovery of three new gas giants, WASP-161 b, WASP-163 b, and WASP-170 b, transiting bright ($V = 11.1$, 12.5, and 12.8) solar-type (F6-, G8-, and G1-type) dwarf stars.

In Section 2, we present the observations used to discover WASP-161 b, WASP-163 b, and WASP-170 b, and to confirm their planetary natures and measure their parameters. In Section 2.2.1, we describe notably TRAPPIST-North, a 60 cm robotic telescope installed recently by the University of Liège at Oukaimeden observatory (Morocco), that played a significant role in the confirmation and characterization of the planets. Section 3.1 presents the determination of the atmospheric parameters of the host stars. In Section 3.2, we describe our global analysis of the data set for the three planetary systems that enabled us to determine their main physical and orbital parameters. We discuss briefly our results in Section 6.

2. Observations and Data Reduction

2.1. WASP Photometry

WASP-161 and WASP-170 (see Table 1 for coordinates and magnitudes) were observed with WASP-South (Hellier et al. 2011, 2012) in 2011 and 2012, while WASP-163 was observed

Table 1

The Parameters of the WASP-161, WASP-163, and WASP-170 Planetary Systems (Values $+1\sigma$ Error Bars), As Deduced from Our Data Analysis Presented in Section 3

| General Star Information | | | |
|---|---|---|---|
| | WASP-161 2MASS08252108–1130035 GaiaId 5751177091580191360 | WASP-163 2MASS17060901–1024467 GaiaId 4334991786994866304 | WASP-170 2MASS09013992–2043133 GaiaId 5656184406542140032 |
| R.A. (J200) | 08 ^h 25 ^m 21 ^s .09 | 17 ^h 06 ^m 08 ^s .98 | 09 ^h 01 ^m 39 ^s .93 |
| Decl. (J200) | −11°30′03″.6 | −10°24′47″.0 | −20°43′13″.6 |
| Vmag [UCAC4] | 10.98 | 12.54 | 12.65 |
| Jmag [2MASS] | 10.09 | 10.67 | 11.13 |
| Gmag [Gaia-DR1] | 10.84 | 12.13 | 12.36 |
| Parallax [mas] [Gaia-DR2] | 2.8864 ± 0.0345 | 3.7981 ± 0.0525 | 3.2439 ± 0.0390 |
| Stellar parameters from spectroscopic analysis | | | |
| T_{eff} (K) | 6400 ± 100 | 5500 ± 200 | 5600 ± 150 |
| $\log g_*$ [cgs] | 4.5 ± 0.15 | 4.0 ± 0.3 | 4.0 ± 0.2 |
| [Fe/H] | +0.16 ± 0.09 | −0.34 ± 0.21 | +0.22 ± 0.09 |
| Spectral type | F6 | G8 | G1 |
| $V \sin i$ [Km/s] | 18 ± 0.8 | <5 | 5.6 ± 1 |
| $\log A(\text{Li})$ | No Lithium seen | <1.6 | 1.52 ± 0.09 |
| Parameters from MCMC analysis | | | |
| MCMC Jump Parameters | | | |
| $(R_p/R_*)^2$ [%] | 0.45092 ± 0.00023 | 1.417 ± 0.067 | 1.382 ± 0.001 |
| Impact parameter b [R_*] | 0.14 ^{+0.15} _{−0.10} | 0.45 ^{+0.09} _{−0.06} | 0.689 ± 0.021 |
| Transit duration W [day] | 0.2137 ± 0.0022 | 0.093 ± 0.001 | 0.085 ± 0.001 |
| Midtransit T_0 [HJD] | 7416.5289 ± 0.0011 | 7918.4620 ± 0.0004 | 7802.3915 ± 0.0002 |
| Orbital period P [day] | 5.4060425 ± 0.0000048 | 1.6096884 ± 0.0000015 | 2.34478022 ± 0.0000036 |
| RV K_2 [m s ^{−1} d ^{1/3}] | 405 ± 20 | 386.69 ± 16 | 340 ± 20 |
| Effective temperature T_{eff} [K] | 6406 ± 100 | 5499 ± 200 | 5593 ± 150 |
| Metallicity [Fe/H] | 0.16 ± 0.09 | −0.34 ± 0.21 | 0.21 ± 0.19 |
| Deduced Stellar Parameters from MCMC | | | |
| Mean density ρ_* [ρ_\odot] | 0.282 ^{+0.013} _{−0.027} | 0.92 ^{+0.13} _{−0.10} | 1.121 ^{+0.093} _{−0.076} |
| Stellar surface gravity $\log g_*$ [cgs] | 4.111 ^{+0.023} _{−0.033} | 4.411 ^{+0.042} _{−0.040} | 4.466 ± 0.031 |
| Stellar mass M_* [M_\odot] | 1.39 ± 0.14 | 0.97 ± 0.15 | 0.93 ± 0.15 |
| Stellar radius R_* [R_\odot] | 1.712 ^{+0.083} _{−0.072} | 1.015 ^{+0.071} _{−0.074} | 0.938 ^{+0.056} _{−0.061} |
| Luminosity L_* [L_\odot] | 4.44 ^{+0.56} _{−0.48} | 0.84 ^{+0.20} _{−0.17} | 0.77 ± 0.14 |
| Deduced Planet Parameters from MCMC | | | |
| | WASP-161 b | WASP-163 b | WASP-170 b |
| RV K [ms ^{−1}] | 230 ± 12 | 329 ± 14 | 255 ± 15 |
| Planet/star radius ratio R_p/R_* | 0.0671 ± 0.0017 | 0.119 ± 0.003 | 0.1175 ± 0.0041 |
| Impact parameter b [R_*] | 0.14 ^{+0.15} _{−0.10} | 0.448 ^{+0.063} _{−0.094} | 0.689 ± 0.021 |
| Semimajor axis a/R_* | 8.49 ^{+0.13} _{−0.28} | 5.62 ^{+0.26} _{−0.21} | 7.71 ^{+0.21} _{−0.18} |
| Orbital semimajor axis a [au] | 0.0673 ± 0.0023 | 0.0266 ± 0.0014 | 0.0337 ± 0.0018 |
| Inclination i_p [deg] | 89.01 ^{+0.69} _{−1.0} | 85.42 ^{+1.10} _{−0.85} | 84.87 ± 0.28 |
| Density ρ_p [ρ_{Jup}] | 1.66 ± 0.22 | 1.07 ^{+0.23} _{−0.17} | 1.21 ^{+0.24} _{−0.19} |
| Surface gravity $\log g_p$ [cgs] | 3.69 ^{+0.37} _{−0.42} | 3.52 ± 0.05 | 3.54 ± 0.05 |
| Mass M_p [M_{Jup}] | 2.49 ± 0.21 | 1.87 ± 0.21 | 1.6 ± 0.2 |
| Radius R_p [R_{Jup}] | 1.143 ^{+0.065} _{−0.058} | 1.202 ± 0.097 | 1.096 ± 0.085 |
| Roche limit a_R [au] | 0.01101 ^{+0.00075} _{−0.00068} | 0.011 ± 0.001 | 0.011 ± 0.001 |
| a/a_R | 6.12 ^{+0.25} _{−0.28} | 2.35 ^{+0.16} _{−0.13} | 3.15 ± 0.19 |
| Equilibrium temperature T_{eq} [K] | 1557 ⁺³⁴ _{−29} | 1638 ± 68 | 1422 ± 42 |
| Irradiation [erg s ^{−1} cm ^{−2}] | 1.35 ^{+0.34} _{−0.26} × 10 ⁹ | 1.63 ± 0.45 × 10 ⁹ | 9.3 ^{+2.3} _{−2.5} × 10 ⁸ |

in 2010 and 2012. The WASP-South data reduction methods described by Collier Cameron et al. (2006) and selected (Collier Cameron et al. 2007) as valuable candidates showing possible transits of short-period (~ 5.4 , 1.6, and 2.3 days) planetary sized bodies (Figure 1).

2.2. Follow-up Photometry

2.2.1. TRAPPIST-North

TRAPPIST-North is a new robotic telescope that is 60 cm in diameter and was installed in 2016 June at the Oukaimeden

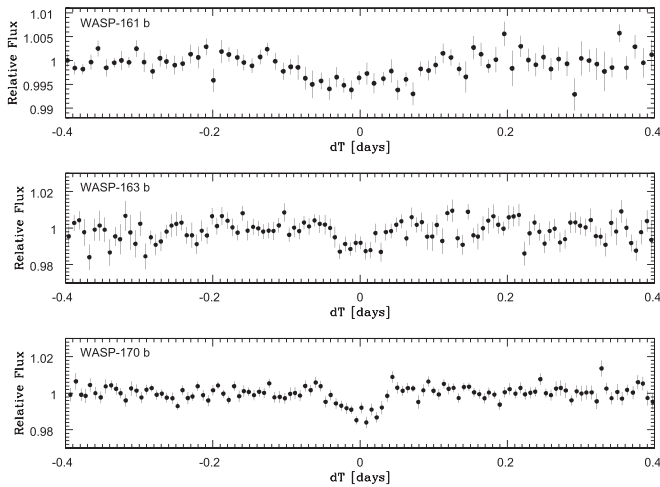


Figure 1. Light curves of WASP-161 (top), WASP-163 (middle), and WASP-170 (bottom) (binned = 10 minutes) folded on the transit ephemeris from the transit search algorithm described in Collier Cameron et al. (2006).

Observatory (Morocco). It was installed by the University of Liège (Belgium) and in collaboration with the Cadi Ayyad University of Marrakech (Morocco). TRAPPIST-North extends the TRAPPIST project to the northern hemisphere, and, like its southern twin TRAPPIST-South, aims to detect and characterize transiting exoplanets and to study comets and other small bodies (e.g., asteroids) in the solar system. The exoplanet program of TRAPPIST (75% of its observational time) is dedicated to several programs: participating in the SPECULOOS project that aims to explore the nearest ultracool dwarf stars for transiting terrestrial planets (Burdanov et al. 2017; Gillon et al. 2017; Delrez et al. 2018; Gillon 2018); the search for the transit of planets previously detected by radial velocity (Bonfils et al. 2011); the follow-up of transiting planets of high interest (e.g., Gillon et al. 2012); and the follow-up of transiting planet candidates identified by wide-field transit surveys like WASP (e.g., Delrez et al. 2014). TRAPPIST-North has an F/8 Ritchey–Chrétien optical design and is protected by a 4.2 m diameter dome equipped with a weather station and independent rain and light sensors. The telescope is equipped with a thermoelectrically cooled 2048×2048 deep-depletion Andor IKONL BEX2 DD CCD camera that has a pixel scale of $0''.60$ that translates into an FOV of $19'.8 \times 19'.8$. It is coupled with a direct-drive mount of German equatorial design. For more technical details and performances of the TRAPPIST telescopes, see Jehin et al. (2011).

TRAPPIST-North observed two partial transits of WASP-161 b in the Sloan- z' filter (2017 December 20 and 2018 February 12), two partial transits and one full transit of WASP-163 b in the $I + z$ filter (2017 April 24, May 2, and June 13), and three partial transits of WASP-170 b in the $I + z$ (2017 April 19 and 2018 January 11) and V (2017 February 17) filters. The reduction and photometric analysis of the data were performed as described in Gillon et al. (2013). The resulting light curves are shown in Figures 2–4.

2.2.2. TRAPPIST-South

We used the 60 cm robotic telescope TRAPPIST-South (TRansiting Planets and PlanetesImals Small Telescope; Gillon et al. 2011; Jehin et al. 2011) at La Silla (Chile) to observe a partial transit of WASP-161 b in the Sloan- z' filter on 2016

January 28, two partial transits of WASP-163 b in a broad $I + z$ filter on 2014 September 6 and 2016 July 5, and two transits (one full + one partial) of WASP-170 b in $I + z$ on 2015 December 25 and 2017 February 26. TRAPPIST-South is equipped with a thermoelectrically cooled $2\text{ K} \times 2\text{ K}$ CCD with the pixel scale of $0''.65$ that translates into a $22' \times 22'$ of FOV. Standard calibration of the images, fluxes extraction, and differential photometry were then performed as described in Gillon et al. (2013). The resulting light curves are shown in Figures 2–4.

2.2.3. EulerCam

We used the EulerCam camera (Lendl et al. 2012) on the 1.2 m Euler-Swiss telescope at La Silla Observatory in Chile to observe a transit of WASP-163 b on 2016 July 27 in the RG filter, and also a transit of WASP-170 b on 2016 December 20 in the broad NGTS filter ($\lambda_{\text{NGTS}} = [500\text{--}900\text{ nm}]$; Wheatley et al. 2018). The calibration and photometric reduction (aperture + differential photometry) of the images were performed as described by Lendl et al. (2012). The resulting light curves are shown in Figures 3 and 4.

2.2.4. NITES

We use 0.4 m NITES (Near-Infrared Transiting Exoplanet Telescope, McCormac et al. 2014) robotic telescope at La Palma (Canary Islands) to observe two transits of WASP-163 b. The first transit was full and observed in R -band on 2016 June 27, while the second was only partial and observed in I -band on 2016 July 10. NITES is equipped with a 1024×1024 CCD camera that has a pixel scale of $0''.66$ that translates into an FOV of $11'.3 \times 11'.3$. The standard calibration of the science images, fluxes extraction, and differential photometry were then performed as described in Craig et al. (2015), Barbary (2016), Bertin & Arnouts (1996), and McCormac et al. (2013). The resulting light curves are shown in Figure 3.

2.2.5. SPECULOOS-South

We use 1 m robotic SSO-Europa telescope, one of the four telescopes of the SPECULOOS-South facility, (more details found in Delrez et al. 2018; Gillon 2018; Burdanov et al. 2017) to observe one full-transit of WASP-161 b on 2018 January 5 in the Sloan- z' filter. Each 1 m robotic telescope is equipped with a $2\text{ K} \times 2\text{ K}$ CCD camera, with good sensitivity in the very-near-infrared up to $1\text{ }\mu\text{m}$. The calibration and photometric reduction of the data were performed as described in Gillon et al. (2013). The resulting light curve is shown in Figure 2.

2.3. Follow-up Spectroscopy

We gathered a series of spectra of the three stars with the CORALIE spectrograph (Queloz et al. 2000) mounted on the 1.2 m Euler-Swiss telescope at ESO La Silla Observatory in Chile. An exposure time of 30 minutes was used for each of these spectroscopic observations. We measured 24 spectra of WASP-161 between 2014 December and 2017 January; 25 spectra of WASP-163 between 2015 June and 2017 May; and 20 spectra of WASP-170 between 2015 February and 2017 May. We applied the cross-correlation technique described in Baranne et al. (1996) on the spectra of each star to measure the radial velocities (RVs) presented in Table 6. The resulting RV time-series shows clear sinusoidal signals with periods and

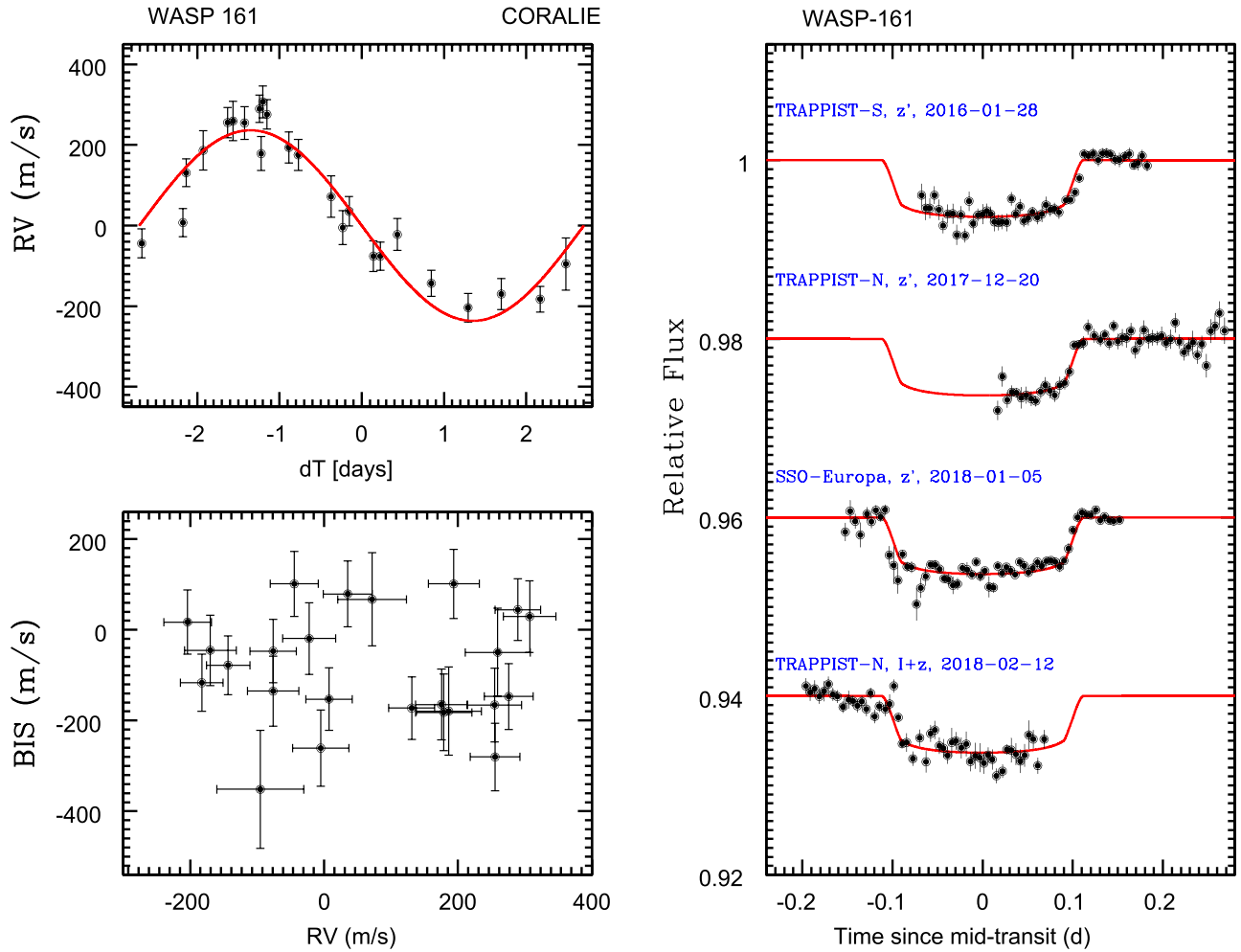


Figure 2. Right panel: individual follow-up transit light curves for WASP-161 binned per 0.005 day (7.2 minutes). The solid red lines are the best-fit transit models. We shifted the light curves along the y axis for clarity. Left panel, top: CORALIE RVs for WASP-161 with the best-fit Keplerian model in red. Left panel, bottom: bisector spans (BIS) vs. RVs diagram.

phases in good agreement with those deduced from the WASP transit detections (Figures 2–4).

For each star, the bisector spans (BSs; Queloz et al. 2001) of the cross-correlation functions (CCF) have standard deviations close to their average errors (122 versus 80 ms^{-1} , 116 versus 125 ms^{-1} , and 87 versus 97 ms^{-1} for WASP-161, WASP-163, and WASP-170 respectively). Furthermore, a linear regression analysis does not show any significant correlation between these BSs and the corresponding RVs, the computed slopes being -0.02 ± 0.16 , 0.07 ± 0.09 , and 0.01 ± 0.11 for, respectively, WASP-161, WASP-163, and WASP-170 (Figures 2–4). This absence of correlation enables us to discard the scenario of a blended eclipsing binary (BEB). Indeed, if the orbital signal of a BEB was causing a clear periodic wobble of the sum of its CCF (s) and that of the target, then it should also create a significant periodic distortion of its shape, resulting in variations of the BS in phase with those of the RV, and with the same order of magnitude (Torres et al. 2004).

3. Data Analysis

3.1. Spectroscopic Analysis

For each host star, we coadded the CORALIE spectra to produce a combined spectrum with an average S/N per pixel

between 50 and 100. We analyzed each combined spectrum with the technique described by Doyle et al. (2013) to determine the following stellar atmospheric parameters: the effective temperature T_{eff} , the surface gravity $\log g$, the lithium abundance $\log A(\text{Li})$, the metallicity $[\text{Fe}/\text{H}]$, and the projected rotational velocity $v \sin i$. $v \sin i$ was constrained using the calibration of Doyle et al. (2014), assuming macroturbulence values of 5.31 km s^{-1} , 3.59 km s^{-1} , and 3.74 km s^{-1} for WASP-161, WASP-163, and WASP-170 respectively. The results of this spectral analysis are shown in Table 1.

3.2. RVs + Light-curves Analysis

We performed a global analysis of the RVs (Table 6) and transit light curves (Table 3) with the MCMC (Markov chain Monte Carlo) algorithm described by Gillon et al. (2012) to determine the parameters of each planetary system. While the CORALIE RVs were modeled with a classical Keplerian model (e.g., Murray & Correia 2010), the transit light curves were represented by the transit model of Mandel & Agol (2002), assuming a quadratic limb-darkening law, multiplied by a baseline model consisting of a polynomial function of one or several external parameters (time, background, airmass, etc.; see Table 3). The selection of the model used for each time-series

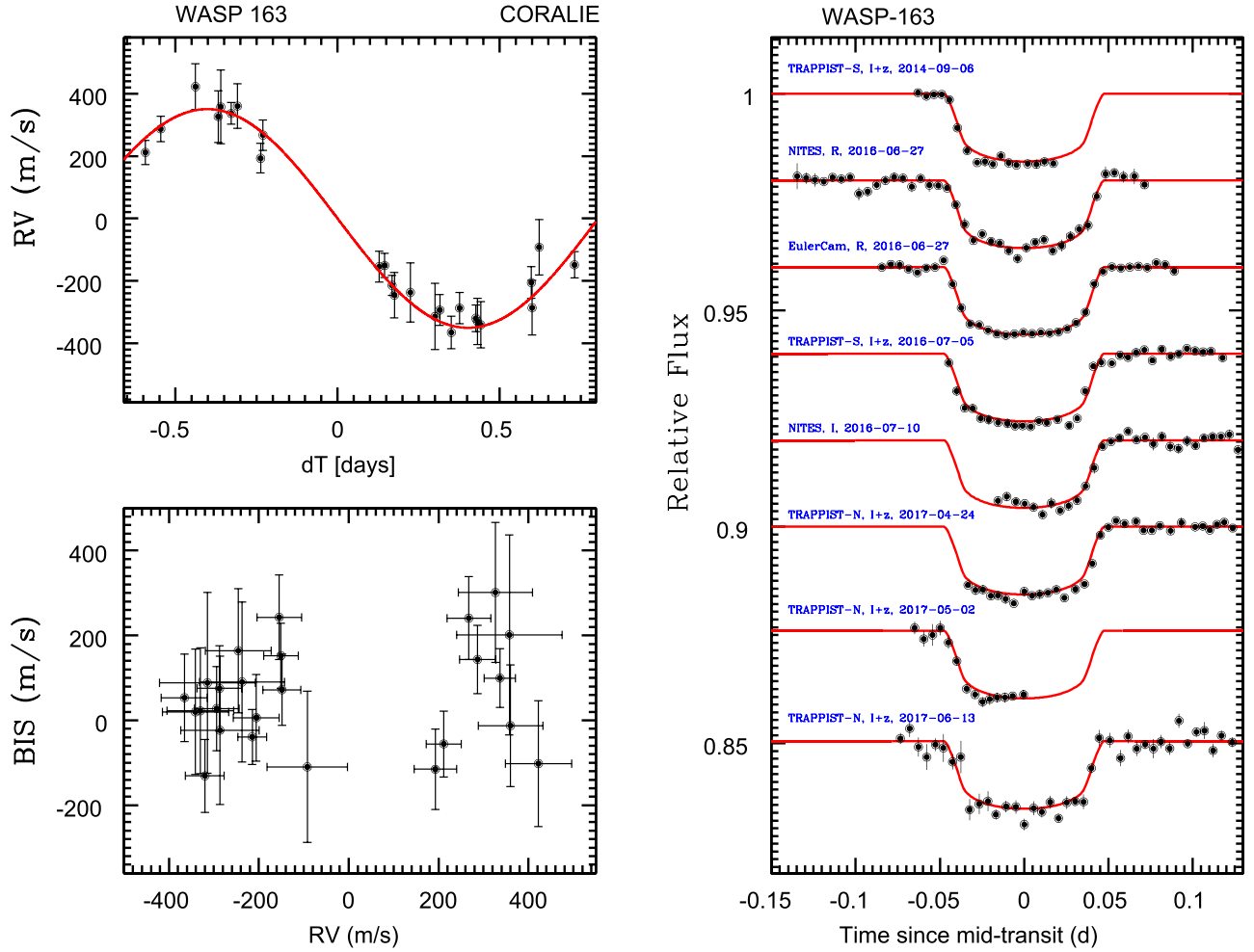


Figure 3. Same as Figure 2 but for WASP-163.

was based on the minimization of the Bayesian Information Criterion (BIC, Schwarz 1978).

TRAPPIST-North and TRAPPIST-South telescopes are equipped with German equatorial mounts that have to rotate 180° at meridian, resulting in different positions of the stars' images on the detector after the flip, translating into an offset of the fluxes in the light curves. For the corresponding light curves, a normalization offset at the time of the flip was thus added to the assumed model (Table 3).

For each system, the “jump” parameters of the Markov Chains, i.e., the parameters perturbed at each step of the chains, were the transit duration, depth, and impact parameter (W , dF , and b , respectively), the orbital period P , the midtransit time T_0 , the parameters $\sqrt{e} \cos \omega$ and $\sqrt{e} \sin \omega$ (with ω the argument of periastron and e the orbital eccentricity), the parameter $K2 = K\sqrt{1 - e^2 P^{1/3}}$ (with K is the RV semiamplitude), and the stellar metallicity $[\text{Fe}/\text{H}]$ and effective temperature T_{eff} . In addition, for each filter, the combinations, $c_1 = 2 \times u_1 + u_2$ and $c_2 = u_1 - 2 \times u_2$ were also jump parameters, u_1 and u_2 being the linear and quadratic limb-darkening coefficients. Normal prior probability distribution functions (PDFs) based on the theoretical tables of Claret (2000) were assumed for u_1 and u_2 (Table 5). For T_{eff} and $[\text{Fe}/\text{H}]$, Gaussian PDFs based on the values + errors derived from our spectral analysis (Table 1) were used. For the other jump parameters, uniform prior PDFs were assumed (e.g., $e \geq 0$, $b \geq 0$).

Each global analysis was composed of three Markov chains of 10^5 steps whose convergence was checked using the statistical test presented by Gelman & Rubin (1992). The correlation of the noise present in the light curves was taken into account by rescaling the errors as described by Gillon et al. (2012). For the RVs, the quadratic difference between the mean error of the measurements and the standard deviation of the best-fit residuals were computed as 32.6 m s^{-1} , 54.1 m s^{-1} , and 42.8 m s^{-1} for WASP-161, WASP-163, and WASP-170, respectively. These “jitter” noises were added quadratically to the errors.

At each step of the Markov chains, a value for the stellar density ρ_* was computed from dF , b , W , P , $\sqrt{e} \cos \omega$, and $\sqrt{e} \sin \omega$ (see, e.g., Winn 2010). This value of ρ_* was then used in combination with the values for T_{eff} and $[\text{Fe}/\text{H}]$ to compute a value for the stellar mass M_* from the empirical calibration of Enoch et al. (2010). Two MCMC analyses were performed for each system, one assuming an eccentric orbit and one assuming a circular one. The Bayes factors, computed as $\exp(-\Delta\text{BIC}/2)$, were largely (>1000) in favor of a circular model for the three systems, and we thus adopted the circular solution for all of them. These solutions are presented in Table 1. The noncircular solutions enable us to estimate the 3σ upper limits on the orbital eccentricity as 0.43, 0.13, and 0.23 for, respectively, WASP-161 b, WASP-163 b, and WASP-170 b.

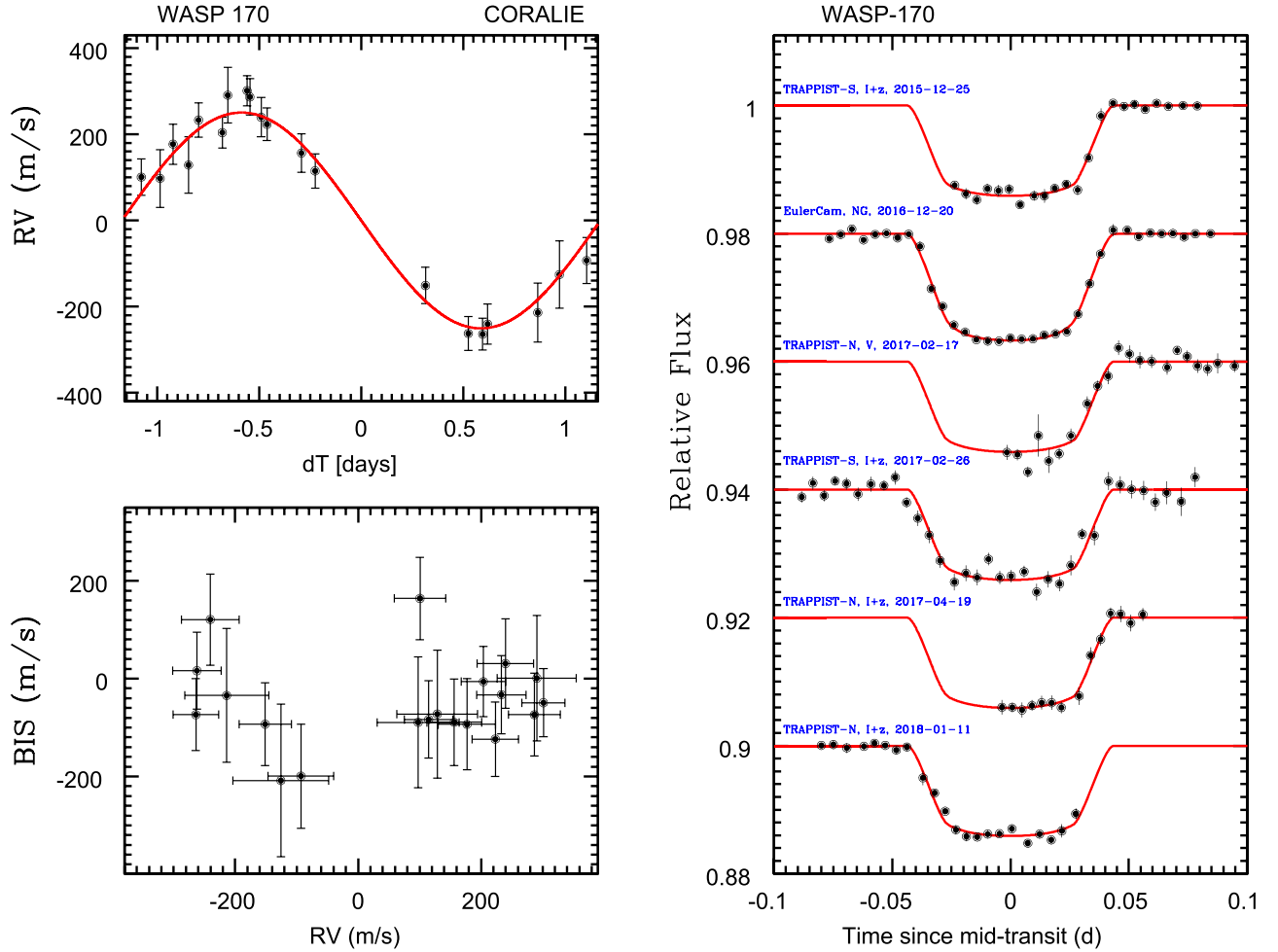


Figure 4. Same as Figure 2 but for WASP-170.

As a sanity check of our results, we also estimated the stellar radius R_* from the star's parallax determined by *Gaia* (Gaia Collaboration et al. 2018), its effective temperature T_{eff} , and its bolometric magnitude M_{bol} , using the equations:

$$M_V = V_{\text{mag}} - 5 \log_{10}(d/10), \quad (1)$$

$$M_{\text{bol}} = M_V + \text{BC}, \quad (2)$$

$$L_*/L_\odot = 10^{0.4(4.74 - M_{\text{bol}})}, \quad (3)$$

$$R_* = L_*/4\pi\sigma T_{\text{eff}}^4, \quad (4)$$

where M_V is the absolute visual magnitude, BC is the bolometric correction (Pecaut & Mamajek 2013), d is the distance in parsec, pc , L_* is the star luminosity, and σ is the Stefan–Boltzmann constant. We estimated the error on R_* by propagating the errors of all other parameters. We obtained $1.55 \pm 0.08 R_\odot$ for WASP-161, $0.86 \pm 0.07 R_\odot$ for WASP-163, and $0.91 \pm 0.06 R_\odot$ for WASP-170, in good agreement with our MCMC results shown in Table 1.¹²

4. Stars' Rotation Periods

The WASP-170 light curve from WASP-South shows a quasi-periodic modulation with an amplitude of about 0.6%

¹² Our photometric and radial-velocity data will be available on the website, <http://cdsarc.u-strasbg.fr>.

| Camera | Dates (JD-2450000) | N | P (day) | a (mmag) | FAP |
|--------|-----------------------|------|-----------|------------|------------|
| 227 | 4846–4943 | 4899 | 7.780 | 0.010 | $<10^{-4}$ |
| 227 | 5567–5675 | 2407 | 3.978 | 0.005 | 0.15 |
| 227 | 5913–6041 | 2794 | 7.725 | 0.007 | $<10^{-4}$ |
| 228 | 4846–4943 | 5283 | 7.703 | 0.011 | $<10^{-4}$ |
| 228 | 5212–5308 | 4747 | 7.813 | 0.006 | 0.002 |
| 228 | 5613–5676 | 2651 | 4.073 | 0.003 | 1.00 |
| 228 | 5913–6041 | 3649 | 7.747 | 0.008 | $<10^{-4}$ |

Note. N : the number of observations used in our analysis, a : the semiamplitude of the best-fit sine wave at the period P found in the periodogram with FAP.

and a period of about 7.8 days. We assume this is due to the star spots (i.e., the combination of the star rotation and the magnetic activity). The rotational modulation of each star was estimated by using the sine-wave fitting method described in Maxted et al. (2011). The star variability due to star spots is not expected to be coherent on long timescales as a consequence of the finite lifetime of the star spots and differential rotation in the photosphere, so we analyzed the WASP-170 data separately. We separately analyzed the WASP-170 data from each camera used, so that we could estimate the reliability of the results. The transit signal was removed from the data to

Table 3
Parameters of Each Light Curve

| Target | Night | Telescope | Filter | N_p | T_{exp} (s) | Baseline function | σ (%) | $\sigma_{7.2 \text{ m}}$ (%) | β_w | β_r | CF |
|----------|-------------|------------|-------------|-------|----------------------|-------------------|--------------|------------------------------|-----------|-----------|------|
| WASP-161 | 2016 Jan 28 | TRAPPIST-S | Sloan- z' | 938 | 10 | $p(t + xy + o)$ | 0.37 | 0.051 | 1.29 | 1.08 | 1.39 |
| WASP-161 | 2017 Dec 20 | TRAPPIST-N | Sloan- z' | 902 | 10 | $p(t + b)$ | 0.43 | 0.072 | 1.14 | 1.05 | 1.20 |
| WASP-161 | 2018 Jan 5 | SPECULOOS | Sloan- z' | 1235 | 10 | $p(xy)$ | 0.44 | 0.087 | 1.22 | 1.44 | 1.72 |
| WASP-161 | 2018 Feb 12 | TRAPPIST-N | Sloan- z' | 892 | 10 | $p(a)$ | 0.46 | 0.054 | 1.14 | 1.20 | 1.37 |
| WASP-163 | 2014 Sep 6 | TRAPPIST-S | $I + z$ | 345 | 12 | $p(t)$ | 0.33 | 0.006 | 1.06 | 1.00 | 1.06 |
| WASP-163 | 2016 Jun 27 | NITES | Johnson-R | 443 | 30 | $p(t)$ | 0.41 | 0.012 | 1.71 | 1.00 | 1.71 |
| WASP-163 | 2016 Jun 27 | EulerCam | RG | 170 | 60 | $p(t + f + b)$ | 0.11 | 0.005 | 1.20 | 1.10 | 1.31 |
| WASP-163 | 2016 Jul 5 | TRAPPIST-S | $I + z$ | 602 | 12 | $p(a + xy)$ | 0.35 | 0.011 | 1.16 | 1.35 | 1.56 |
| WASP-163 | 2016 Jul 10 | NITES | Johnson-I | 388 | 30 | $p(t)$ | 0.58 | 0.012 | 1.55 | 1.18 | 1.83 |
| WASP-163 | 2017 Apr 24 | TRAPPIST-N | $I + z$ | 487 | 12 | $p(t + xy + o)$ | 0.31 | 0.008 | 1.02 | 1.07 | 1.09 |
| WASP-163 | 2017 May 2 | TRAPPIST-N | $I + z$ | 213 | 12 | $p(b)$ | 0.54 | 0.009 | 0.90 | 1.00 | 0.90 |
| WASP-163 | 2017 Jun 13 | TRAPPIST-N | $I + z$ | 557 | 14 | $p(t + f)$ | 0.69 | 0.021 | 0.87 | 1.16 | 1.01 |
| WASP-170 | 2015 Dec 25 | TRAPPIST-S | $I + z$ | 359 | 15 | $p(f)$ | 0.29 | 0.008 | 1.04 | 1.05 | 1.09 |
| WASP-170 | 2016 Dec 20 | EulerCam | NGTS | 207 | 40 | $p(t)$ | 0.11 | 0.005 | 1.49 | 1.13 | 1.68 |
| WASP-170 | 2017 Feb 17 | TRAPPIST-N | Johnson-V | 239 | 20 | $p(t)$ | 0.46 | 0.013 | 1.22 | 1.00 | 1.22 |
| WASP-170 | 2017 Feb 26 | TRAPPIST-S | $I + z$ | 545 | 15 | $p(t + a)$ | 0.51 | 0.015 | 1.32 | 1.16 | 1.53 |
| WASP-170 | 2017 Apr 19 | TRAPPIST-N | $I + z$ | 186 | 15 | $p(a + xy)$ | 0.41 | 0.008 | 0.99 | 1.00 | 0.99 |
| WASP-170 | 2018 Jan 11 | TRAPPIST-N | $I + z$ | 315 | 15 | $p(t)$ | 0.26 | 0.007 | 0.75 | 1.11 | 0.83 |

Note. The table shows for each light curve the date, telescope, filter, number of data points, exposure time, selected baseline function, rms of the best-fit residuals, deduced values for β_w , β_r and CF = $\beta_w \times \beta_r$. For the baseline function, $p(\epsilon^N)$, denotes, respectively, an N -order polynomial function of time ($\epsilon = t$), airmass ($\epsilon = a$), full width at half maximum ($\epsilon = f$), background ($\epsilon = b$), and x and y positions ($\epsilon = xy$). The symbol o denotes an offset fixed at the time of the meridian flip.

Table 4
Stellar Mass and Age Estimates from the Software *BAGEMASS*

| Star | Mass [M_\odot] | Age [Gyr] |
|------------|------------------------|------------------------------------|
| WASP-161 A | 1.42 ± 0.05 (1.40) | 2.4 ± 0.4 (2.4) |
| WASP-163 A | 0.87 ± 0.06 (0.78) | 11.4 ± 3.5 (17.4) ^a |
| WASP-170 A | 0.99 ± 0.07 (1.03) | 4.8 ± 3.1 (2.9) |

Note.

^a Best fit occurs at edge of model grid.

Table 5
The Quadratic Limb-darkening (LD) Coefficients u_1 and u_2 Used in Our MCMC Analysis

| LD Coefficient | WASP-161 | WASP-163 | WASP-170 |
|-------------------|-------------------|-------------------|---------------------|
| $u_{1,z'}$ | 0.184 ± 0.011 | ... | ... |
| $u_{2,z'}$ | 0.300 ± 0.005 | ... | ... |
| $u_{1,I+z}$ | ... | 0.207 ± 0.012 | 0.2539 ± 0.0202 |
| $u_{2,I+z}$ | ... | 0.297 ± 0.010 | 0.2788 ± 0.0152 |
| $u_{1,Johnson-I}$ | ... | 0.331 ± 0.034 | 0.2727 ± 0.0321 |
| $u_{2,Johnson-I}$ | ... | 0.251 ± 0.019 | 0.2805 ± 0.0158 |
| $u_{1,Johnson-R}$ | ... | 0.420 ± 0.043 | ... |
| $u_{2,Johnson-R}$ | ... | 0.248 ± 0.027 | ... |
| $u_{1,Johnson-V}$ | ... | ... | 0.437 ± 0.044 |
| $u_{2,Johnson-V}$ | ... | ... | 0.271 ± 0.025 |

calculate the periodograms by subtracting a simple transit model from the light curve. We calculated the periodograms over uniformly spaced frequencies from 0 to 1.5 cycles/day. The false alarm probability (FAP) is calculated by the bootstrap Monte Carlo as described in Maxted et al. (2011). The results are presented in Table 2, and the periodograms and light curves are shown in Figure 5. The rotation period value we obtain is $P_{\text{rot}} = 7.75 \pm 0.02$ days from the clear signal near 7.8 days in five out of seven data sets. From the stellar radius estimated and the rotation period, the value of $V_{\text{rot}} \sin I = 6.1 \pm 0.3 \text{ km s}^{-1}$ is implied, assuming that the

axes of the star and the planet orbital are approximately aligned, in good agreement with our spectroscopic analysis ($v \sin i = 5.6 \pm 1.0 \text{ km s}^{-1}$, see the Table 1). We modeled the rotational modulation in the light curves for each camera and season with the rotation period fixed at $P_{\text{rot}} = 7.75$ days using the least-squares fit of a sinusoidal function and its first harmonic. Similar analyses are performed for WASP-161 and WASP-163.

5. Stellar Evolution Modeling

We estimated the mass and age of the host stars using the software *BAGEMASS*¹³ based on the Bayesian method described in Maxted et al. (2015). The models used in the software *BAGEMASS* were calculated using the *GARSTEC* stellar evolution code as described in Weiss & Schlattl (2008). The deduced stellar masses and ages calculated are shown in Table 4. The inferred masses are in good agreement with the ones resulting from our global MCMC analysis (see Table 1).

6. Discussion

WASP-161 b, WASP-163 b, and WASP-170 b are planets slightly larger ($1.14 \pm 0.06 R_{\text{Jup}}$, $1.2 \pm 0.1 R_{\text{Jup}}$, and $1.10 \pm 0.09 R_{\text{Jup}}$) and more massive ($2.5 \pm 0.2 M_{\text{Jup}}$, $1.9 \pm 0.2 M_{\text{Jup}}$, and $1.6 \pm 0.2 M_{\text{Jup}}$) than Jupiter. Given their masses and their large irradiations (Figure 6(a)), their radii are well reproduced by the models of Fortney et al. (2007), assuming a core mass of a few dozens of M_\oplus and ages larger than a few hundreds of megayears (Figure 6(b)).

The empirical relationship derived by Weiss et al. (2013) for planets more massive than $150 M_\oplus$, $R_p/R_\oplus = 2.45 (M_p/M_\oplus)^{-0.039 \pm 0.01} (F/\text{erg s}^{-1} \text{ cm}^{-2})^{0.094}$ predicts radii of $1.16 \pm 0.30 R_{\text{Jup}}$, $1.20 \pm 0.34 R_{\text{Jup}}$, and $1.15 \pm 0.31 R_{\text{Jup}}$ for WASP-161 b, 163 b, and 170 b, respectively, which are consistent with our measured radii. The three new planets

¹³ <http://sourceforge.net/projects/bagemass>

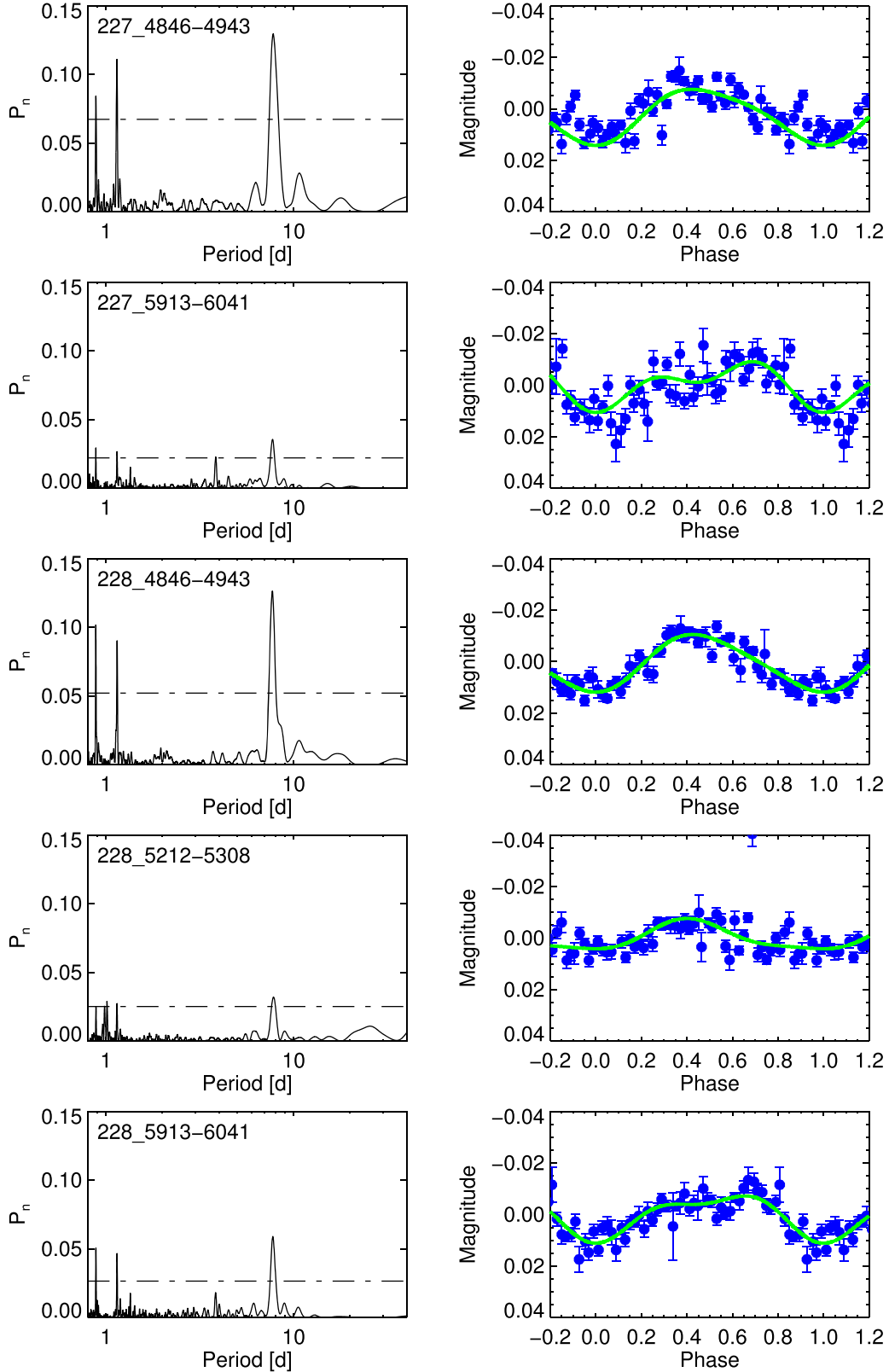


Figure 5. Left panel: periodograms of WASP-170. Horizontal lines indicate FAP levels 0.1, 0.01, and 0.001. Right panel: light curves binned in the blue points on the assumed rotation period of 7.75 days with second-order harmonic series fit by least squares in the green lines.

whose discovery is described thus appear to be “standard” hot Jupiters that do not present a “radius anomaly” challenging standard models of irradiated gas giants.

The discovery of WASP-161 b, WASP-163 b, and WASP-170 b establishes the new robotic telescope TRAPPIST-North as a powerful northern facility for the photometric follow-up of

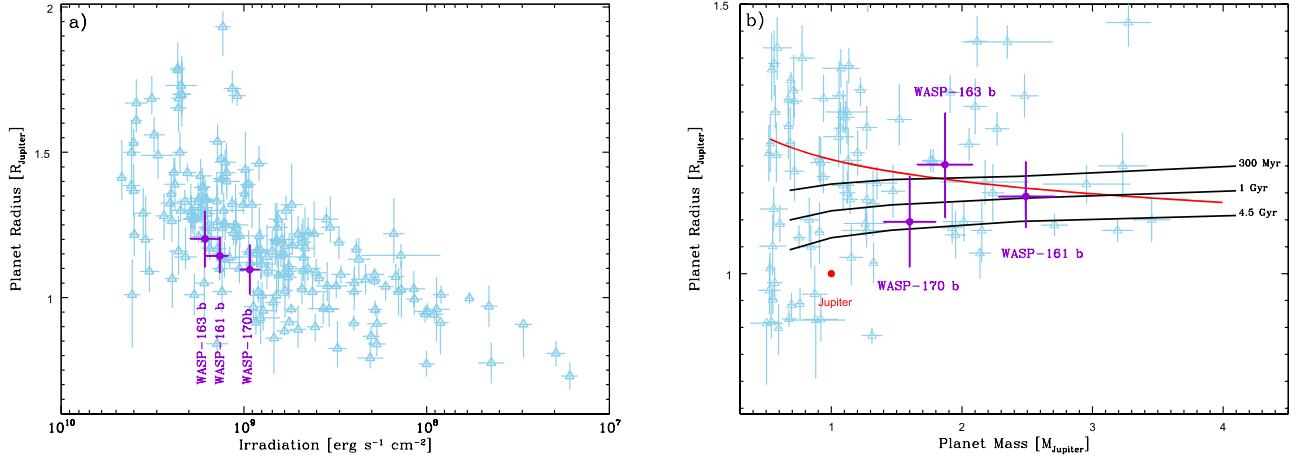


Figure 6. Panel (a): irradiation-radius diagram. Panel (b): mass-radius diagram for the known transiting planets with masses ranging from 0.5 to 4 M_{Jupiter} (data from exoplanets.org are shown as skyblue triangles with error bars). The planets WASP-161 b, WASP-163 b, and WASP-170 b are shown in violet. In (b), the black lines present models of irradiated giant planets with semimajor axes of 0.045 au, core masses of 25 M_{\oplus} , and ages of 300 Myr, 1 Gyr and 4.5 Gyr (Fortney et al. 2007). The empirical law of Weiss et al. (2013) is also plotted as a red line.

Table 6
CORALIE Radial-velocity Measurements for WASP-161, WASP-163, and WASP-170 (BS = bisector spans)







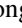





| Target | HJD- 2,450,000 | RV (km s ⁻¹) | σ_{RV} (km s ⁻¹) | BS (km s ⁻¹) | Target | HJD- 2,450,000 | RV (km s ⁻¹) | σ_{RV} (km s ⁻¹) | BS (km s ⁻¹) |
|----------|-------------------|-----------------------------|---|-----------------------------|----------|-------------------|-----------------------------|---|-----------------------------|
| WASP-163 | 7193.741864 | -37.28368 | 0.11764 | -0.05553 | WASP-161 | 6995.779435 | 37.47673 | 0.03954 | 0.10140 |
| WASP-163 | 7194.544082 | -37.93075 | 0.07383 | 0.14349 | WASP-161 | 7404.735111 | 37.93140 | 0.04051 | -0.15260 |
| WASP-163 | 7221.642393 | -37.90136 | 0.07320 | -0.10196 | WASP-161 | 7421.604076 | 37.83967 | 0.03886 | -0.17254 |
| WASP-163 | 7264.560197 | -37.21532 | 0.08258 | 0.30132 | WASP-161 | 7422.600890 | 37.60262 | 0.03490 | -0.17929 |
| WASP-163 | 7265.528948 | -37.85780 | 0.08717 | 0.20131 | WASP-161 | 7423.668930 | 37.52064 | 0.03555 | -0.28021 |
| WASP-163 | 7268.579849 | -37.96344 | 0.07401 | 0.09958 | WASP-161 | 7425.646222 | 37.72356 | 0.03456 | -0.04948 |
| WASP-163 | 7276.497340 | -37.95927 | 0.10641 | -0.01258 | WASP-161 | 7426.579130 | 37.96837 | 0.03946 | -0.16563 |
| WASP-163 | 7277.497313 | -37.30844 | 0.07177 | -0.11522 | WASP-161 | 7428.627488 | 37.41733 | 0.03252 | 0.04443 |
| WASP-163 | 7292.517764 | -37.82511 | 0.09442 | 0.24068 | WASP-161 | 7451.572650 | 37.47357 | 0.03171 | -0.18188 |
| WASP-163 | 7293.464761 | -37.14368 | 0.07405 | 0.24267 | WASP-161 | 7452.635935 | 37.57245 | 0.03459 | 0.02944 |
| WASP-163 | 7294.524814 | -37.73113 | 0.08910 | 0.15248 | WASP-161 | 7453.567361 | 37.93838 | 0.03395 | -0.14701 |
| WASP-163 | 7484.863204 | -37.46746 | 0.03879 | -0.03903 | WASP-161 | 7457.538982 | 37.46129 | 0.03590 | 0.10144 |
| WASP-163 | 7486.827998 | -37.42444 | 0.04741 | 0.16399 | WASP-161 | 7481.604825 | 37.65253 | 0.04218 | -0.16457 |
| WASP-163 | 7487.796538 | -37.79839 | 0.04198 | 0.09038 | WASP-161 | 7485.611602 | 37.80633 | 0.03723 | 0.06739 |
| WASP-163 | 7488.843232 | -37.86941 | 0.03227 | 0.08838 | WASP-161 | 7669.874869 | 37.96450 | 0.03643 | -0.26075 |
| WASP-163 | 7523.858463 | -37.41079 | 0.04884 | 0.02768 | WASP-161 | 7670.873488 | 37.54791 | 0.03644 | 0.07926 |
| WASP-163 | 7567.695488 | -37.80440 | 0.03823 | 0.05318 | WASP-161 | 7674.868344 | 37.89486 | 0.04877 | -0.13512 |
| WASP-163 | 7569.757824 | -37.85478 | 0.05104 | 0.07520 | WASP-161 | 7716.752403 | 37.48642 | 0.06487 | -0.04681 |
| WASP-163 | 7575.726750 | -37.81565 | 0.04977 | -0.13093 | WASP-161 | 7717.747923 | 37.75662 | 0.04854 | -0.01920 |
| WASP-163 | 7576.662344 | -37.38270 | 0.04033 | 0.02235 | WASP-161 | 7718.788841 | 37.80035 | 0.03818 | -0.07805 |
| WASP-163 | 7577.523403 | -37.95890 | 0.04961 | 0.01980 | WASP-161 | 7726.778064 | 37.39224 | 0.03876 | 0.01718 |
| WASP-163 | 7593.681424 | -37.95775 | 0.05024 | 0.00629 | WASP-161 | 7746.846331 | 37.51936 | 0.03845 | -0.04507 |
| WASP-163 | 7652.535369 | -37.33184 | 0.03470 | -0.02346 | WASP-161 | 7751.735303 | 37.69111 | 0.05137 | -0.11653 |
| WASP-163 | 7823.841592 | -38.04752 | 0.05155 | -0.10981 | WASP-161 | 7761.696319 | 37.93171 | 0.04203 | -0.35162 |
| WASP-163 | 7894.742995 | -37.97268 | 0.04302 | 0.07214 | | | | | |
| WASP-170 | 7066.749515 | 30.67098 | 0.04671 | 0.16402 | WASP-170 | 7753.676136 | 30.70862 | 0.03924 | -0.12366 |
| WASP-170 | 7686.843189 | 31.25138 | 0.06427 | -0.08954 | WASP-170 | 7754.698984 | 31.19850 | 0.04009 | -0.08925 |
| WASP-170 | 7694.846421 | 30.81621 | 0.04224 | -0.09353 | WASP-170 | 7759.695126 | 31.20223 | 0.04579 | -0.08356 |
| WASP-170 | 7719.778573 | 31.25569 | 0.04232 | -0.07239 | WASP-170 | 7760.780900 | 30.70044 | 0.03683 | -0.09317 |
| WASP-170 | 7721.746763 | 31.13284 | 0.04660 | -0.03291 | WASP-170 | 7773.792434 | 31.17400 | 0.03803 | 0.01621 |
| WASP-170 | 7723.773046 | 30.84403 | 0.05319 | -0.00621 | WASP-170 | 7801.545185 | 31.08175 | 0.06548 | -0.07362 |
| WASP-170 | 7724.787756 | 31.05367 | 0.03945 | 0.00095 | WASP-170 | 7812.635803 | 30.67711 | 0.06835 | 0.12073 |
| WASP-170 | 7726.799025 | 31.25678 | 0.03495 | -0.04931 | WASP-170 | 7825.546120 | 31.14228 | 0.04425 | -0.03448 |
| WASP-170 | 7747.780705 | 31.16081 | 0.03596 | -0.07385 | WASP-170 | 7859.637199 | 30.88820 | 0.07800 | -0.20830 |
| WASP-170 | 7749.729288 | 31.01646 | 0.04208 | 0.03075 | WASP-170 | 7883.473343 | 31.07842 | 0.06692 | -0.19927 |

transiting exoplanet candidates found by ground-based wide-field surveys like WASP, and soon by the space-based mission *TESS* (Ricker et al. 2016).

WASP-South is hosted by the SAAO and we are grateful for their ongoing support and assistance. Funding for WASP comes from consortium universities and from the UK's Science

and Technology Facilities Council. The Euler-Swiss telescope is supported by the Swiss National Science Foundation. TRAPPIST-South is funded by the Belgian Fund for Scientific Research (FNRS) under the grant FRFC 2.5.594.09.F, with the participation of the Swiss National Science Foundation (SNF). M.G. is FNRS Research Associate, and E.J. is FNRS Senior Research Associate. L.D. acknowledges support from the Gruber Foundation Fellowship. The research leading to these results has received funding from the European Research Council under the FP/2007-2013 ERC Grant Agreement 336480, and from the ARC grant for Concerted Research Actions, financed by the Wallonia-Brussels Federation. This work was also partially supported by a grant from the Simons Foundation (ID 327127 to Didier Queloz), a grant from the Erasmus+ International Credit Mobility programme (K. Barkaoui), as well as by the MERAC foundation (P. I. Triaud).

ORCID iDs

A. Burdanov  <https://orcid.org/0000-0001-9892-2406>
 C. Hellier  <https://orcid.org/0000-0002-3439-1439>
 M. Gillon  <https://orcid.org/0000-0003-1462-7739>
 B. Smalley  <https://orcid.org/0000-0002-3456-087X>
 P. F. L. Maxted  <https://orcid.org/0000-0003-3794-1317>
 M. Lendl  <https://orcid.org/0000-0001-9699-1459>
 A. H. M. J. Triaud  <https://orcid.org/0000-0002-5510-8751>
 D. J. Armstrong  <https://orcid.org/0000-0002-5080-4117>
 A. C. Cameron  <https://orcid.org/0000-0002-8863-7828>
 D. Pollacco  <https://orcid.org/0000-0001-9850-9697>
 F. J. Pozuelos  <https://orcid.org/0000-0003-1572-7707>
 D. Queloz  <https://orcid.org/0000-0002-3012-0316>

References

- Baranne, A., Queloz, D., Mayor, M., et al. 1996, *A&AS*, **119**, 373
 Barbary, K. 2016, *JOSS*, **1**, 58
 Bertin, E., & Arnouts, S. 1996, *A&AS*, **117**, 393
 Bonfils, X., Gillon, M., Forveille, T., et al. 2011, *A&A*, **528**, A111
 Burdanov, A., Delrez, L., Gillon, M., Jehin, E., & Speculoos, T. 2017, in *Handbook of Exoplanets*, ed. H. J. Deeg & J. A. Belmonte (Berlin: Springer), 130
 Chang, C., Liu, G. Z., Tang, C. X., et al. 2010, *ApPhL*, **96**, 111502
 Charbonneau, D., Brown, T. M., Latham, D. W., & Mayor, M. 2000, *ApJL*, **529**, L45
 Claret, A. 2000, *yCat*, **336**, 1081
 Collier Cameron, A., Pollacco, D., Street, R. A., et al. 2006, *MNRAS*, **373**, 799
 Collier Cameron, A., Wilson, D. M., West, R. G., et al. 2007, *MNRAS*, **380**, 1230
 Correia, A. C. M., & Laskar, J. 2010, *Icar*, **205**, 338
 Craig, M. W., Crawford, S. M., Deil, C., et al. 2015, *ccdproc: CCD Data Reduction Software*, Astrophysics Source Code Library, ascl:1510.007
 Crossfield, I. J. M. 2015, *PASP*, **127**, 941
 Delrez, L., Gillon, M., Queloz, D., et al. 2018, *Proc. SPIE*, **10700**, 1070011
 Delrez, L., Van Grootel, V., Anderson, D. R., et al. 2014, *A&A*, **563**, A143
 Deming, D., & Seager, S. 2009, *Natur*, **462**, 301
 Doyle, A. P., Davies, G. R., Smalley, B., Chaplin, W. J., & Elsworth, Y. 2014, *MNRAS*, **444**, 3592
 Doyle, A. P., Smalley, B., Maxted, P. F. L., et al. 2013, *MNRAS*, **428**, 3164
 Enoch, B., Collier Cameron, A., Parley, N. R., & Hebb, L. 2010, *A&A*, **516**, A33
 Fortney, J. J., Marley, M. S., & Barnes, J. W. 2007, *ApJ*, **659**, 1661
 Gaia Collaboration, Brown, A. G. A., Vallenari, A., et al. 2018, *A&A*, **616**, A1
 Gelman, A., & Rubin, D. B. 1992, *StaSe*, **7**, 457
 Gillon, M. 2018, *NatAs*, **2**, 344
 Gillon, M., Anderson, D. R., Collier-Cameron, A., et al. 2013, *A&A*, **552**, A82
 Gillon, M., Jehin, E., Magain, P., et al. 2011, *EPJ Web of Conferences*, **11**, 06002
 Gillon, M., Triaud, A. H. M. J., Demory, B.-O., et al. 2017, *Natur*, **542**, 456
 Gillon, M., Triaud, A. H. M. J., Fortney, J. J., et al. 2012, *A&A*, **542**, A4
 Hellier, C., Anderson, D. R., Collier-Cameron, A., et al. 2011, *ApJL*, **730**, L31
 Hellier, C., Anderson, D. R., Collier Cameron, A., et al. 2012, *MNRAS*, **426**, 739
 Henry, G. W., Marcy, G. W., Butler, R. P., & Vogt, S. S. 2000, *ApJL*, **529**, L41
 Jehin, E., Gillon, M., Queloz, D., et al. 2011, *Msngr*, **145**, 2
 Lendl, M., Anderson, D. R., Collier Cameron, A., et al. 2012, *A&A*, **544**, A72
 Mandel, K., & Agol, E. 2002, *ApJL*, **580**, L171
 Maxted, P. F. L., Anderson, D. R., Collier Cameron, A., et al. 2011, *PASP*, **123**, 547
 Maxted, P. F. L., Serenelli, A. M., & Southworth, J. 2015, *A&A*, **575**, A36
 Mayor, M., & Queloz, D. 1995, *Natur*, **378**, 355
 McCormac, J., Pollacco, D., Skillen, I., et al. 2013, *PASP*, **125**, 548
 McCormac, J., Skillen, I., Pollacco, D., et al. 2014, *MNRAS*, **438**, 3383
 Murray, C. D., & Correia, A. C. M. 2010, in *Exoplanets*, ed. S. Seager (Tucson, AZ: Univ. Arizona Press), 15
 Pecaui, M. J., & Mamajek, E. E. 2013, *ApJS*, **208**, 9
 Pollacco, D. L., Skillen, I., Collier Cameron, A., et al. 2006, *PASP*, **118**, 1407
 Queloz, D., Henry, G. W., Sivan, J. P., et al. 2001, *A&A*, **379**, 279
 Queloz, D., Mayor, M., Naef, D., et al. 2000, in *Proc. ESO Symp., From Extrasolar Planets to Cosmology: The VLT Opening Symp.*, ed. J. Bergeron & A. Renzini (Berlin: Springer-Verlag), 548
 Ricker, G. R., Vanderspek, R., Winn, J., et al. 2016, *Proc. SPIE*, **9904**, 99042B
 Schwarz, G. 1978, *AnSta*, **6**, 461
 Seager, S., & Deming, D. 2010, *ARA&A*, **48**, 631
 Sing, D. K., Fortney, J. J., Nikolov, N., et al. 2016, *Natur*, **529**, 59
 Torres, G., Konacki, M., Sasselov, D. D., & Jha, S. 2004, *ApJ*, **614**, 979
 Weiss, A., & Schlattl, H. 2008, *Ap&SS*, **316**, 99
 Weiss, L. M., Marcy, G. W., Rowe, J. F., et al. 2013, *ApJ*, **768**, 14
 Wheatley, P. J., West, R. G., Goad, M. R., et al. 2018, *MNRAS*, **475**, 4476
 Winn, J. N. 2010, in *Exoplanets*, ed. S. Seager (Tucson, AZ: Univ. Arizona Press), 55
 Winn, J. N., & Fabrycky, D. C. 2015, *ARA&A*, **53**, 409